metals

MDPI

Review

Ultrafast Heating Heat Treatment Effect on the Microstructure and Properties of Steels

Matteo Gaggiotti [1], Luciano Albini [2], Paolo Emilio Di Nunzio [2], Andrea Di Schino [1], Giulia Stornelli [3,*] and Giulia Tiracorrendo [2]

[1] Dipartimento di Ingegneria, Università degli Studi di Perugia, Via G. Duranti 93, 06125 Perugia, Italy
[2] RINA Consulting—Centro Sviluppo Materiali SpA, Via Castel Romano 100, 00128 Roma, Italy
[3] Dipartimento di Ingegneria Industriale, Università degli Studi di Roma "Tor Vergata", Via del Politecnico 1, 00133 Roma, Italy
* Correspondence: giulia.stornelli@students.uniroma2.eu

Abstract: The adoption of the ultrafast heating (UFH) process has gained much attention in the last few years, as the green energy and minimization of CO_2 emissions are the main aspects of contemporary metal science and thermal treatment. The effect of ultrafast heating (UFH) treatment on carbon steels, non-oriented grain (NGO) electrical steels, and ferriticor austenitic stainless steels is reported in this review. The study highlights the effect of ultrarapid annealing on microstructure and textural evolution in relation to microstructural constituents, recrystallization temperatures, and its effect on mechanical properties. A strong influence of the UFH process was reported on grain size, promoting a refinement in terms of both prior austenite and ferrite grain size. Such an effect is more evident in medium–low carbon and NGO steels than that in ferritic/austenitic stainless steels. A comparison between conventional and ultrafast annealing on stainless steels shows a slight effect on the microstructure. On the other hand, an evident increase in uniform elongation was reported due to UFH. Textural evolution analysis shows the effect of UFH on the occurrence of the Goss component (which promotes magnetic properties), and the opposite with the recrystallization g-fiber. The recovery step during annealing plays an important role in determining textural features; the areas of higher energy content are the most suitable for the nucleation of the Goss component. As expected, the slow annealing process promoted equiaxed grains, whereas rapid heating promoted microstructures with elongated grains as a result of the cold deformation.

Keywords: ultrafast heating; heat treatment; carbon steels; stainless steels; NGO steel; microstructure

Citation: Gaggiotti, M.; Albini, L.; Di Nunzio, P.E.; Di Schino, A.; Stornelli, G.; Tiracorrendo, G. Ultrafast Heating Heat Treatment Effect on the Microstructure and Properties of Steels. *Metals* **2022**, *12*, 1313. https://doi.org/10.3390/met12081313

Academic Editor: Andrey Belyakov

Received: 19 July 2022
Accepted: 3 August 2022
Published: 5 August 2022

1. Introduction

In recent years, the application of ultrafast heating (UFH) treatment has gained considerable attention from both the academic and industrial communities [1]. Such a heat treatment is enabled by the possibility to electrically heat metallic materials by an electromagnetic induction process based on Joule heating through heat transfer passing through an induction coil, generating an electromagnetic field. The rapidly alternating magnetic field penetrates the object, generating so-called eddy currents inside the metallic component. Such currents flow through the resistance of the material, thus heating it by the Joule effect. UFH could strongly optimize industrial production processes in terms of time and consequently productivity [2–5]. Results very near to industrial applications were reported by Cola Jr. in AISI 8620 and in bainitic steels [6,7], but the most important limit appears to be related to UFH rates with respect to conventional steel-processing lines [8].

UFH is a process based on induction heating (IH) that is widely used to heat-treat specific areas more rapidly, and at a lower cost and lower amount of energy consumption compared to conventional heat treatment methods [8,9]. The inductive heat treatment offers several advantages over conventional heat treatments using a furnace, such as short

processing times, high flexibility, and localized annealing [10–12]. The temperature variation over time of the annealing process is represented by the parameter of heating rate (HR). Variation in HR affects the phase transformation kinetics and steel properties; an increase in terms of HR raises the α/γ transformation temperature, thus leading to austenitic grain refinement [13–16]. At the same time, an increase in phase transformation temperatures [17] reduces the carbon amount that can be dissolved in austenite, thus lowering steel hardenability [6]. In addition, during fast heating, the solubility of carbonitrides and pearlite areas is also evidently dependent on heating time and not just temperature, as what usually happens in conventional annealing processes [18,19].

Concerning carbon steels, UFH can be adopted in the austenitization process step (before quenching and tempering) [20–29]. In the case of austenitic stainless steels, UFH is a promising method to be applied after cold rolling to promote grain refinement [30], leading to an increase in terms of mechanical properties [31–33].

In carbon steels, the application of UFH inhibits the dislocation rearrangement that is typical of recovery [33–36]. Hence, recrystallization occurs in direct competition with austenitization [37–39]. The final microstructure of a steel subjected to UFH strongly depends on heating rate and peak temperature [40,41]. In the case of a high HR and inadequate peak temperature, a not fully recrystallized microstructure is achieved [42,43]. When conditions instead allow for complete recrystallization, the microstructure shows a morphology resulting in plastic deformation.

Since recovery is usually negligible in the case of austenitic stainless steels, the immediate start of recrystallization during UFH does not imply significant changes in the mechanism [44]. Ferritic stainless steels, instead, show a final microstructure comparable with that of industrial products [45,46], with a fully recrystallized structure and equiaxed grains for appropriate temperatures [47–51].

The aim of this review paper is to highlight trends in variation in the above-mentioned properties with heating rate, and to predict their behavior when possible for different classes of materials, focusing on the main metallurgical topics (phase transformation, recrystallization, and textural evolution).

2. Effect of UFH on Grain Size

In medium/low carbon steels, the application of UFH leads to a significant decrease in grain size due to the suppression of grain boundary movements, and thus the growth of austenite grains [52–58]. Figure 1 shows the prior austenite grain (PAG) size dependence of heating rate (HR) [40]. In the case of 0.25 wt. % C heat-treated specimens with a peak temperature at 850 °C, HR (between 10 and 1000 °C/s) and cooling rate of 20 °C/s, some authors [40] investigated the effect of HR on the variation in ferritic grain size (Figure 2). Results show an evident average PAG size refinement of about 55% (from 3.8 down to 1.7 μm) (Figure 1) that corresponds to a consequent decrease in ferritic grain size (about 20%, from 2.5 to 2 mm) (Figure 2) as the HR increased from 10 up to 1000 °C/s. A similar steel grade (0.2 wt. % C) was considered by Hernandez-Duran et al. [57], who studied the effect of the same HR as that in [40] on the ferritic grain size, and the results, reported in Figure 2, show a similar refinement of ferritic grain size, with a reduction from 2 to 1.6 mm.

Petrov et al. [59] studied the effect of heating rate increase on a cold-rolled high strength carbon steel grade for automotive applications. They indicated that, when varying the heating rate in the range from 140 to 1500 °C/s, ferritic grain refinement was achieved from 4 to 1 μm. They also showed that excellent ultimate tensile strength (higher than 1200 MPa) and acceptable fracture elongation were achieved. The above results were confirmed by an increase in heating rate of up to 1500 °C/s [40] that, compared to 150 °C/s, led to a more pronounced decrease in ferritic grain size of about 76%, from 2.6 to 0.6 μm (Figure 3).

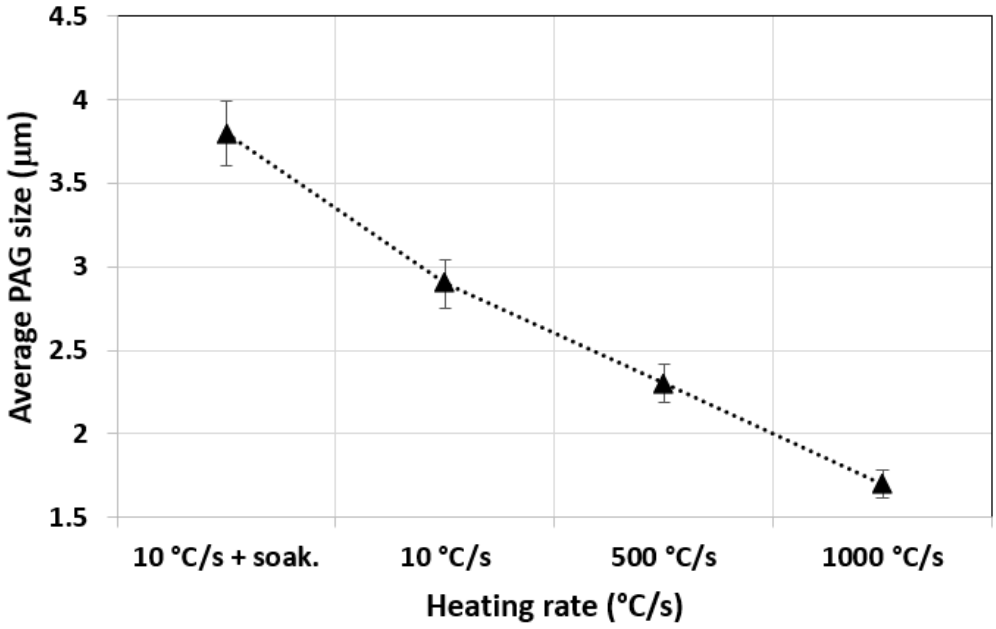

Figure 1. Effect of the heating rate increase on PAG size (data from [40]). Low/medium carbon steel (0.25 wt. % C), peak temperature of 850 °C, and cooling rate of 20 °C/s.

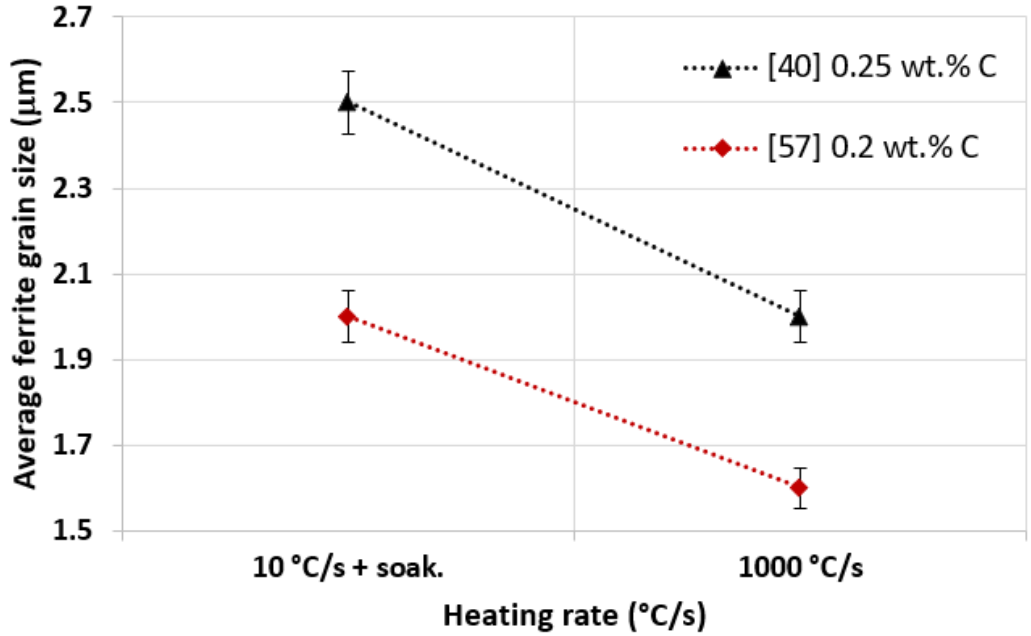

Figure 2. Effect of the heating rate increase on ferritic grain size. Low/medium carbon steel (0.25 wt. % C and 0.2 wt. % C), peak temperature of 850 °C and 950 °C, cooling rate of 20 °C/s and 160 °C/s (data from [40,57]).

An example of microstructures obtained after UFH is reported in Figure 4, referring to the industrial hot-rolled strips of a low-C steel (0.08% C, 0.3% Mn) and of an HSLA steel (0.07% C, 0.5% Mn, 0.03% Nb), cold-rolled from 3 down to 0.5 mm, and processed by imposing different peak temperatures and heating rates to find the optimal processing conditions for achieving full recrystallization. No soaking was applied, and the strips were cooled down just after reaching the peak temperature.

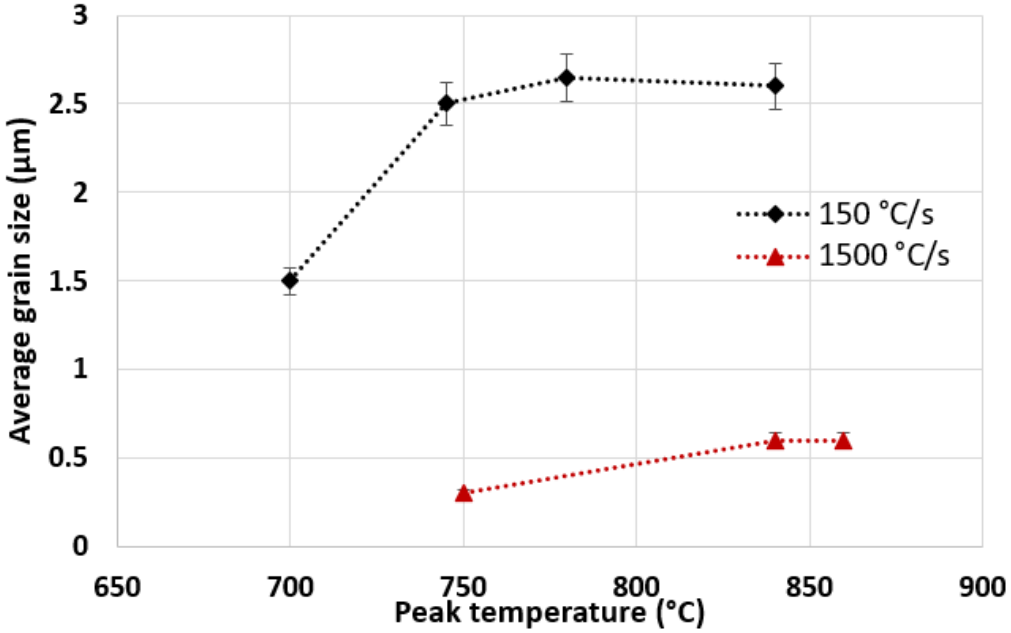

Figure 3. Ferritic grain size variation as function of temperature for the heating rates of 150 and 1500 °C/s (data from [42]).

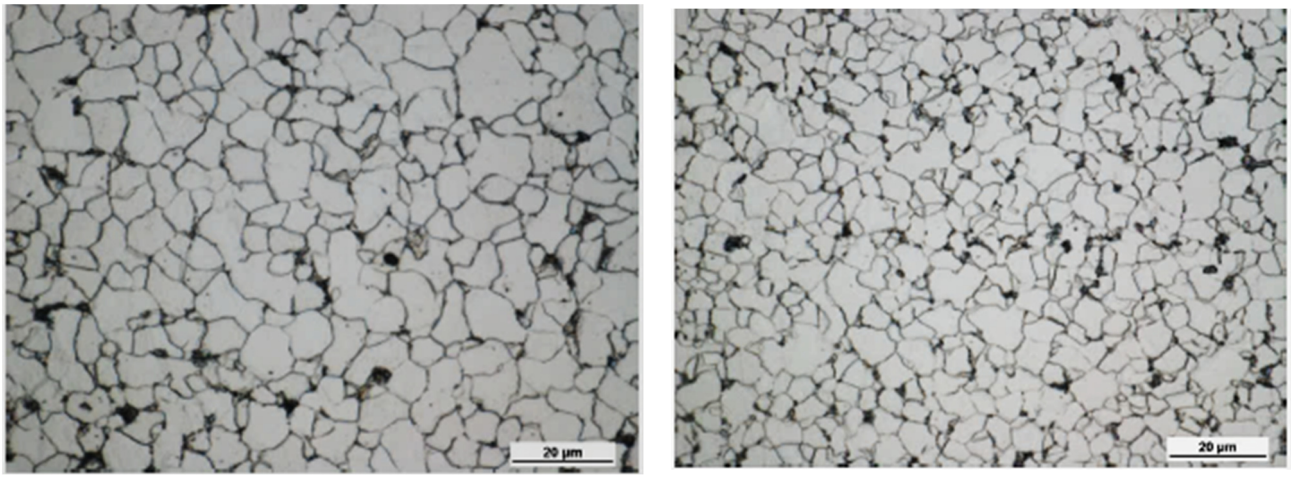

(**a**) (**b**)

Figure 4. Microstructure of fully recrystallized steels subjected to UFH. (**a**) Low-C 0.08% C, 0.3% Mn steel; (**b**) HSLA 0.07% C, 0.5% Mn, 0.03% Nb steel.

The first steel was processed with a peak temperature of 870 °C and a heating rate of 285 °C/s, obtaining an average ferritic grain size of 6.1 µm and a hardness of 136 HV_{300g} (Figure 4a). The second steel was processed with a peak temperature of 820 °C and a heating rate of 325 °C/s, obtaining an average ferritic grain size of 5.4 µm and a hardness of 158 HV_{300g} (Figure 4b). The microstructures appeared to not be very refined, but the resulting tensile properties, nevertheless, complied with grades DX51D and HX340LAD.

If ferritic stainless steels are considered, an increasing heating rate leads to less marked grain refinement, as reported in [45]. Data reported in [45] showed that the average grain size of AISI 430 steel decreased from 7.4 to 6.7 µm for a heating rate of 1000 °C/s. Similarly, Salvatori and Moore [60] analyzed the effect of UFH on AISI 430 ferritic stainless steels, and showed them to be able to reproduce industrial standard products with a heating rate of up 1000 °C/s.

3. Effect of UFH on Ac_1–Ac_3 Temperatures and on Recrystallization Phenomenon

The quantitative effect of heating rate increase on Ac_1 and Ac_3 temperatures is related to the steel chemical composition, and several data are found in the literature showing in many cases an increase in both critical temperatures with increasing heating rate.

In a low/medium carbon steel, Valdes-Tabernero et al. [48] (Figure 5) showed a more pronounced increase in Ac_1 than that in Ac_3 in the range of heating rates from 1 to 200 °C/s. An increase in Si and Mn leads to the opposite effect [38]. In this case, a stronger dependence of Ac_3 temperature on heating rate with respect to Ac_1 was also reported (Figure 6).

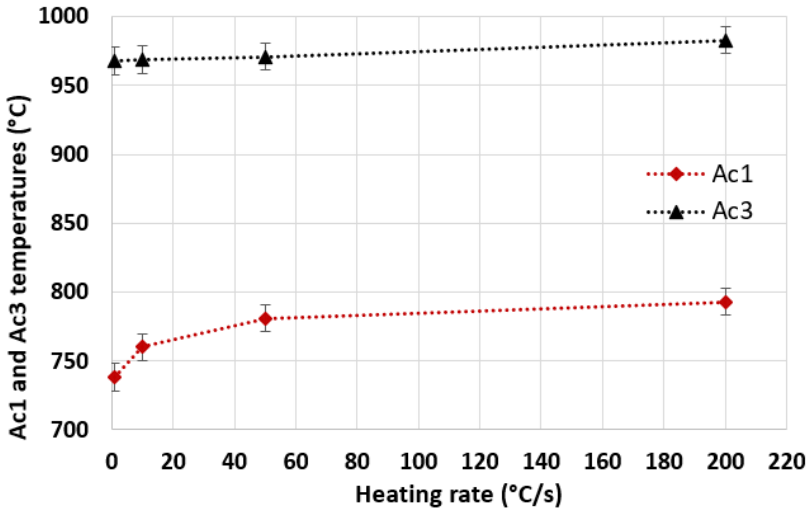

Figure 5. Effect of HV increase on Ac_1 and Ac_3 temperature variation (steel chemical composition 0.19% C + 0.5% Si + 1.61% Mn + 1.06% Al), peak temperature of 1100 °C, and cooling rate of 300 °C/s (data from [48]).

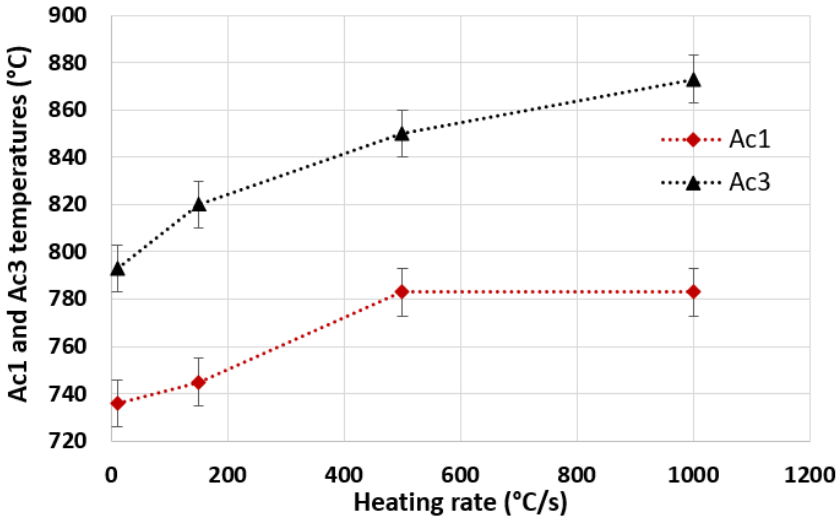

Figure 6. Ac_1 and Ac_3 temperature variation with an increase in HR (steel chemical composition 0.25% C + 1.5% Si + 3.0% Mn) (data from [40]).

Concerning the recrystallization process, the increase in heating rate led to an increase in the recrystallization temperature, supported by the following evidence:

- The recrystallized fraction decreased with increasing heating rate: in a low carbon steel at 750 °C for a heating rate of 150 °C/s, the recrystallized fraction was ~0.5%. At the same temperature for a heating rate of 1500 °C/s, the recrystallized fraction decreased to 0.1% [42]; in [43], compared to a conventional annealing treatment (10 °C/s and

recrystallized fraction of ~77%), during an ultrafast annealing process (778 °C/s), the recrystallized fraction became ~24%.

- In [42], the recrystallized fraction increased with increasing peak temperature: for a peak temperature of 850 °C for two heating rates (150 and 1500 °C/s), the recrystallized fraction was ~0.6% for 150 °C/s and ~0.2% for 1500 °C/s, a value greater than that for 750 °C (Figure 7).
- The recrystallization of ferrite takes place simultaneously with the $\alpha \rightarrow \gamma$ phase transformation [61].

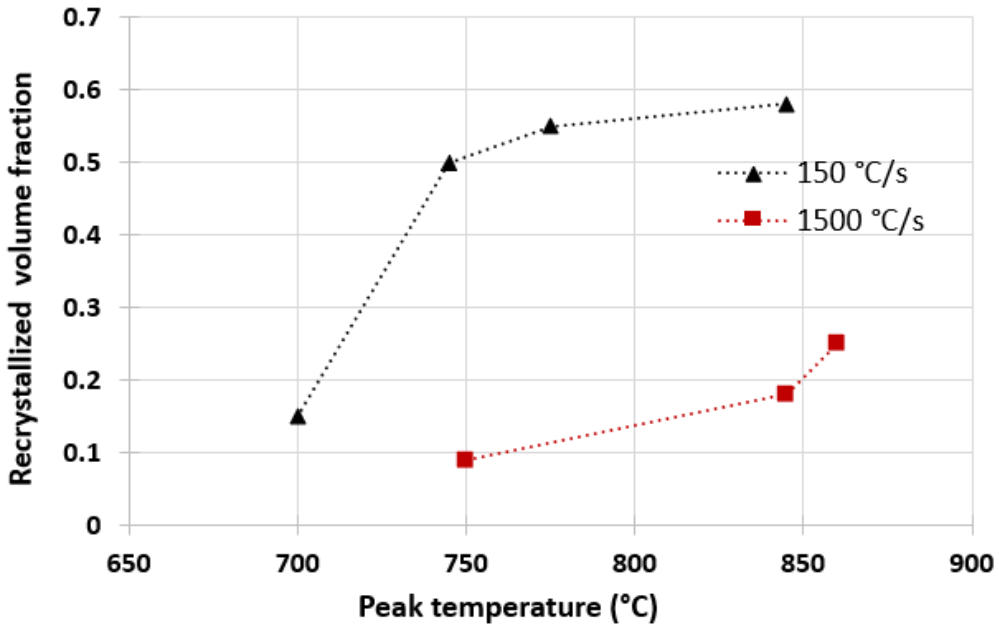

Figure 7. Recrystallized fraction as a function of peak temperature for two different HRs (data from [42]).

4. Effect of UFH on Mechanical Properties

4.1. Carbon Steels

Directly connected to the effect of ultrafast heating on grain size refinement, the mechanical properties of carbon steels subjected to the UFH process showed a clear improvement. Specifically, the evolution of mechanical characteristics was reported for low/medium carbon steel in the case of conventional annealing + soaking (10 °C/s + soak.), conventional annealing (10 °C/s) and ultrafast annealing (500–1000 °C/s) prior to quenching and partitioning (Q and P) heat treatment [40]. Results showed that the Ultimate Tensile Strength (UTS)increased for a higher HR (Figure 8); from conventional annealing (HR of CA = 10 °C/s) to ultrafast heating (HR of UFH = 1000 °C/s), the UTS shifted from 1097 to 1318 MPa (an increase of ~20%). The yield stress (YS), in the same range of heating rate, decreased from 837 to 811 MPa (−3.2%), and uniform elongation ε_c increased from 2.6% to 12.8%.

A comparison of CA (5 °C/s) and UFH (500 °C/s) on dual-phase steel [39] showed the following results: the UTS improved from 625.0 ± 3.6 MPa to 666.0 ± 2.6 MPa (~6.5%), the YS increased from 277.0 ± 8.1 MPa to 372.0 ± 3.0 MPa (~34%), and the uniform elongation and total elongation increased from 16.5 ± 0.2% to 18 ± 0.5% and from 23.3 ± 0.8% to 26.6 ± 0.5%, respectively (Figures 9 and 10).

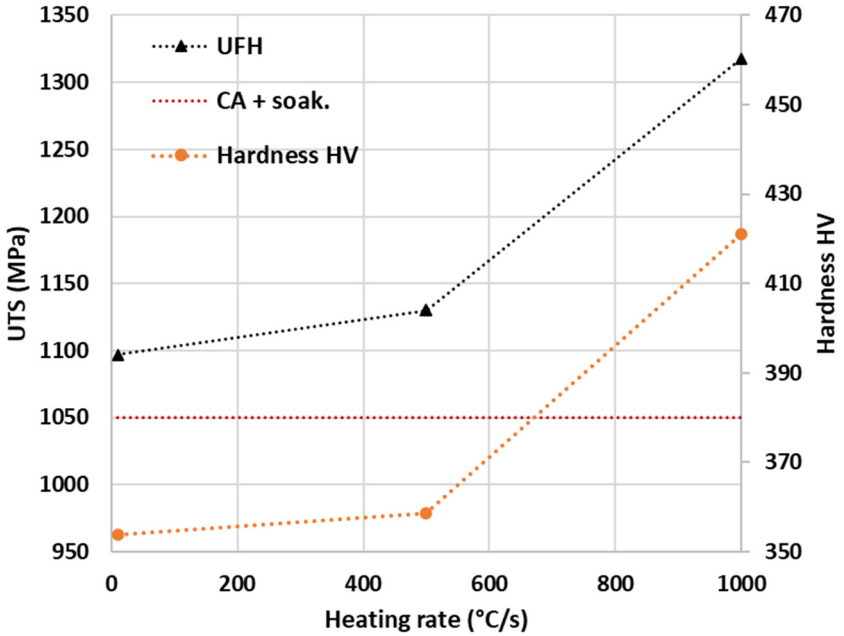

Figure 8. Effect of HR increase on UTS and Vicker hardness value of a low/medium carbon steel undergone the UFH process compared to CA + soaking process (steel chemical composition 0.25% C + 1.5% Si + 3.0% Mn)). Peak temperature of 850 °C, and cooling rate of 20 °C/s (data from [40]).

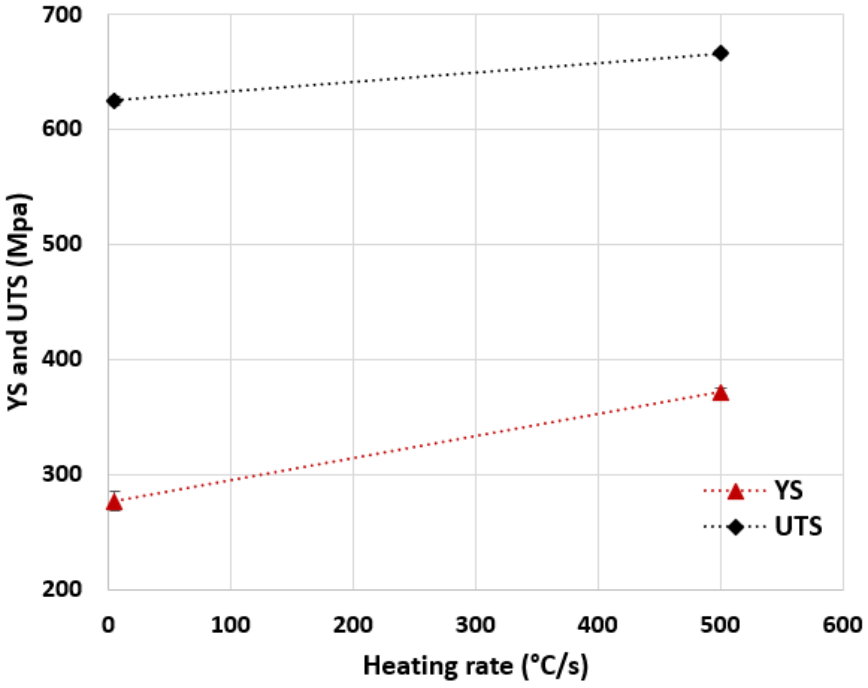

Figure 9. YS and UTS increase with increase in heating rate between CA (5 °C/s) and UFH (500 °C/s), on dual-phase steel (data from [41]).

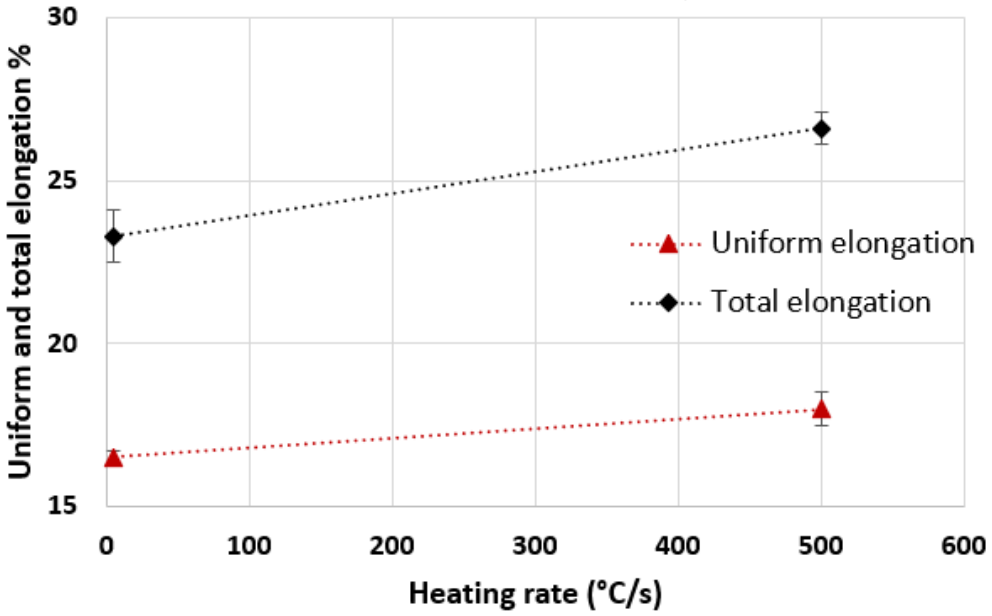

Figure 10. Uniform and total elongation variation with increasing heating rate between CA (5 °C/s) and UFH (500 °C/s) on dual-phase steel (data from [41]).

4.2. Stainless Steels

Regarding the mechanical properties in ferritic stainless steels [60]:

- The values were very similar to those typical of standard industrial production, even if the tensile strength was a little lower. These properties improved as the holding time increased and they did not seem to depend on heating rate. With further increases in holding time, yield stress and tensile strength values remained almost constant, and the total elongation increased.
- A thermal cycle using no holding time in the annealing treatment allowed for obtaining a product that was quite comparable to the industrial standard in the whole range of heating rates (500–1000 °C/s).

Instead, from data reported in [45]:

- The YS, UTS, and ε_c were practically equal for all specimens heated at a peak temperature below 900 °C. At a peak temperature of 900 °C, the yield strength was reduced, even though the grain size and hardness did not change from those at 880 °C.
- As the annealing temperature increased to 900 °C, the yield strength decreased, which is beneficial for formability.

In austenitic stainless steels, data from [44] show that:

- Without any holding time at a peak temperature of 700 °C/s and heating rates of 2 and 20 °C/s, the YS increased to 870 MPa, with an improvement in ductility and uniform elongation (ε_c). Increasing from 2 to 100 °C/s, the UTS and YS did not change too much (UTS from 1013 to 967 MPa and YS from 856 to 778 MPa)), but ductility was improved.
- The uniform elongation was improved from 11% to 37% with the increase in HR from 2 to 100 °C/s.

5. Effect of UFH on Microstructure

The effect of heating rate on the microstructure was clearly reported in [43] for a process involving a heating rate of 778 °C/s in comparison to a standard 10 °C/s heating rate.

The recrystallized volume for a low-carbon steel (0.14 wt. % C), decreased from 77.4% to 27.3%, the fraction of recovered ferrite increased from 8.6% to 54.5%, and the martensite + pearlite fraction increased from 14% to 21.8% (Figure 11).

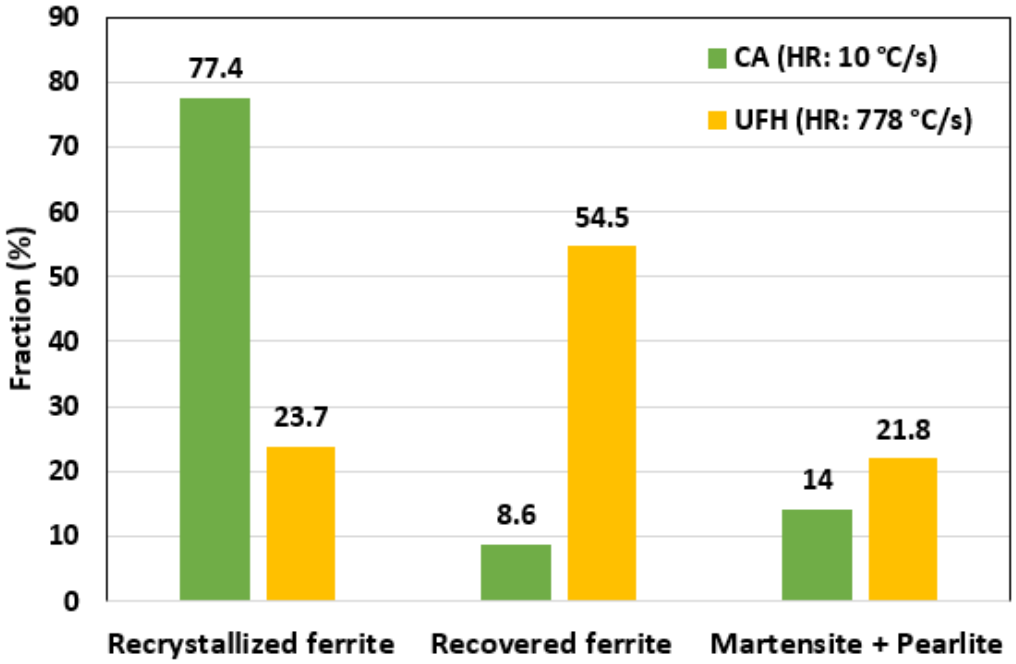

Figure 11. Microstructural evolution for CA (HR: 10 °C/s) and UFH (HR: 778 °C/s), low-carbon steel (0.14% C) (data from [43]).

This result is in contrast with that in [38,39], where an increase in Ac_1 temperature was reported with increasing HR; therefore, less martensite was expected in the microstructure of the UFH sample than that in the CA sample.

The difference can be explained by the lack of ferritic recrystallization in the UFH sample.

A possible explanation of the above results can be that the peak temperature of the specimen treated with CA was lower than that processed by UFH, and that, in the latter treatment, some austenite was formed. In the case of CA, it is reasonable to assume that not only was the peak temperature lower, but also the treatment time at high temperature was longer, so that the recrystallized fraction could be higher than that of the steel treated with UFH. When the steel was cooled, the austenite transformed into martensite.

From the comparison between CA + soaking and UFH prior to Q and P heat treatment [38], for a carbon steel (0.25 wt. % C), the fraction of ferrite increased for higher heating rates from 0% at 10 °C/s + soak. to 25% at 1000 °C/s. This was due to the very short heating time and consequently the absence of complete austenitization. The most important difference from 500 to 1000 °C was the fraction on fresh martensite (15% → 2%) that was replaced by ferrite (5% → 25%) (Figure 12).

Therefore, for this class of steels, UFH heating rates of up to about 500 °C/s are still suitable to achieve a similar microstructure to those of Q and P grades. Instead, for heating rates above 500 °C/s, complex microstructures are produced where ferrite coexists with retained austenite.

The dependence of microconstituent fraction formation as a function of a combination of HR, peak temperature, and steel chemical composition is reported in Figures 13–16 (data from [57]). The comparison is between a low-carbon steel (0.2 wt. % C) and stabilized low-carbon steel (0.2 wt. % C + Mo + Ti + Nb), and the results show that:

- The martensite volume fraction decreased with increasing heating rate (Figures 13 and 14).
- At Ac_3 temperature (Figures 14 and 15), the fraction of martensite showed an opposite trend at 1000 °C/s with respect to lower temperature. This is evidence of the impact of peak temperature on ultrafast heating treatment.
- Concerning the low-C stabilized steel, the effect of alloying elements on hardenability was clear. After UFH at Ac_3 temperature, the fraction of martensite was equal to 100% (Figure 16).

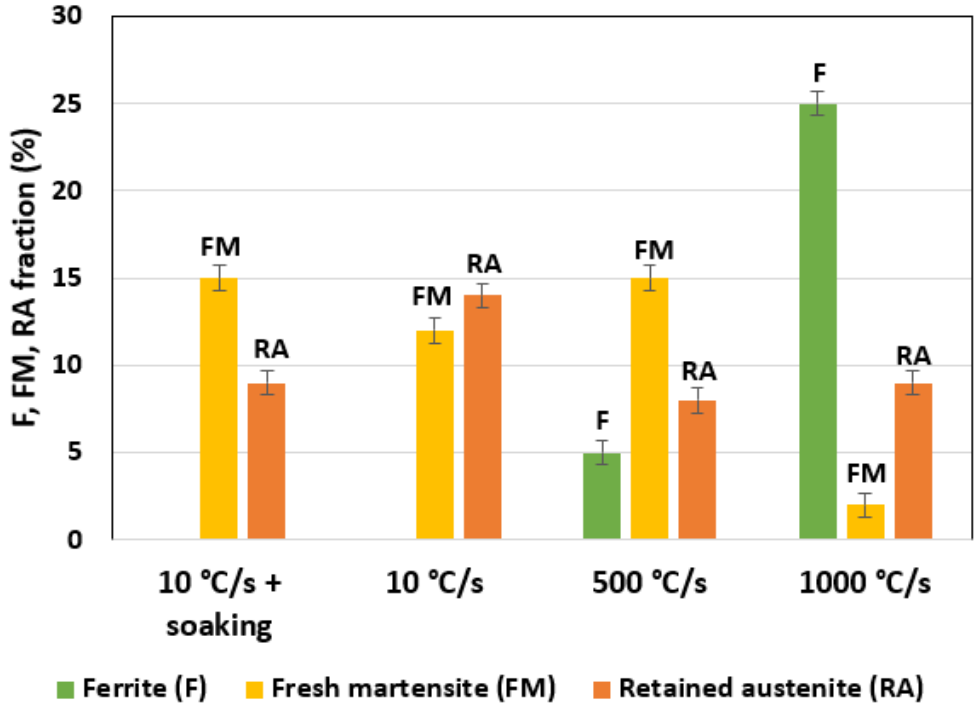

Figure 12. Microstructural evolution for different heating rates (data from [40]; steel chemical composition: 0.25% C + 1.2% Si + 3.0% Mn).

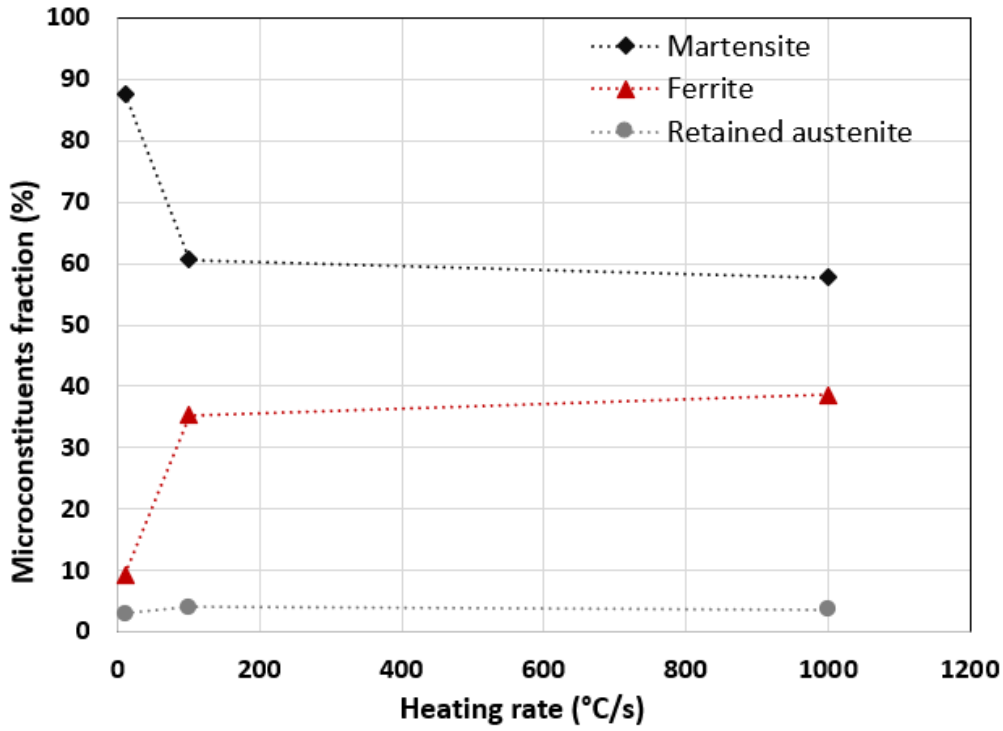

Figure 13. Microstructural evolution at different HRs for peak temperature at 902 °C (data from [57]; steel chemical composition: 0.2% C).

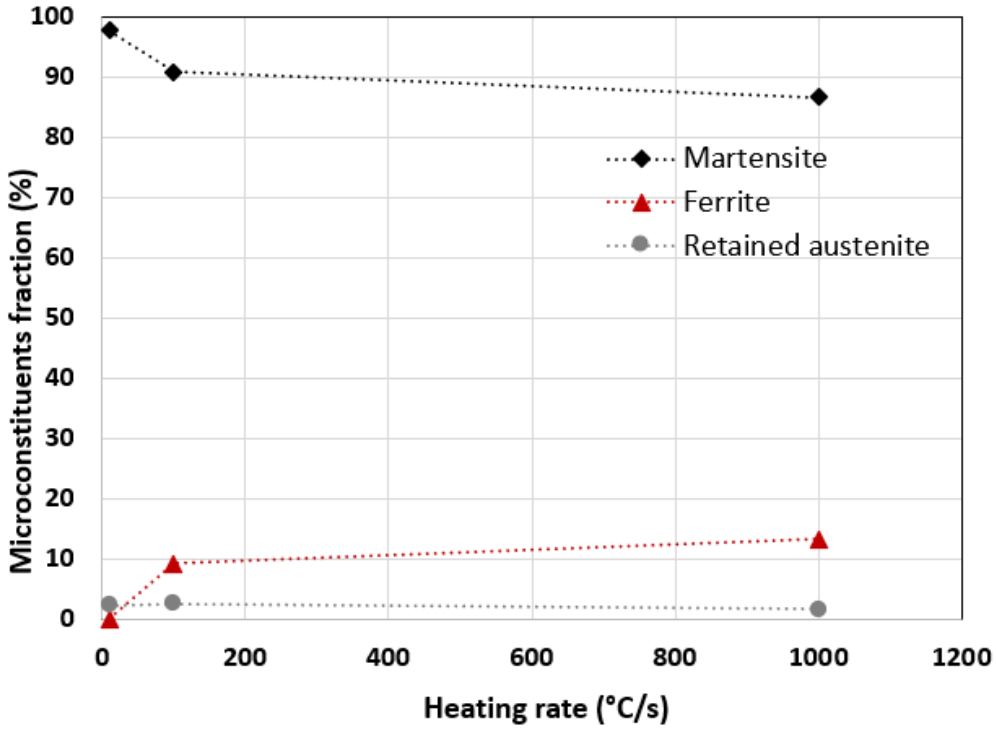

Figure 14. Microstructural evolution at different HRs for peak temperature at 915 °C (data from [57]; steel chemical composition: 0.2% C + Mo + Ti + Nb).

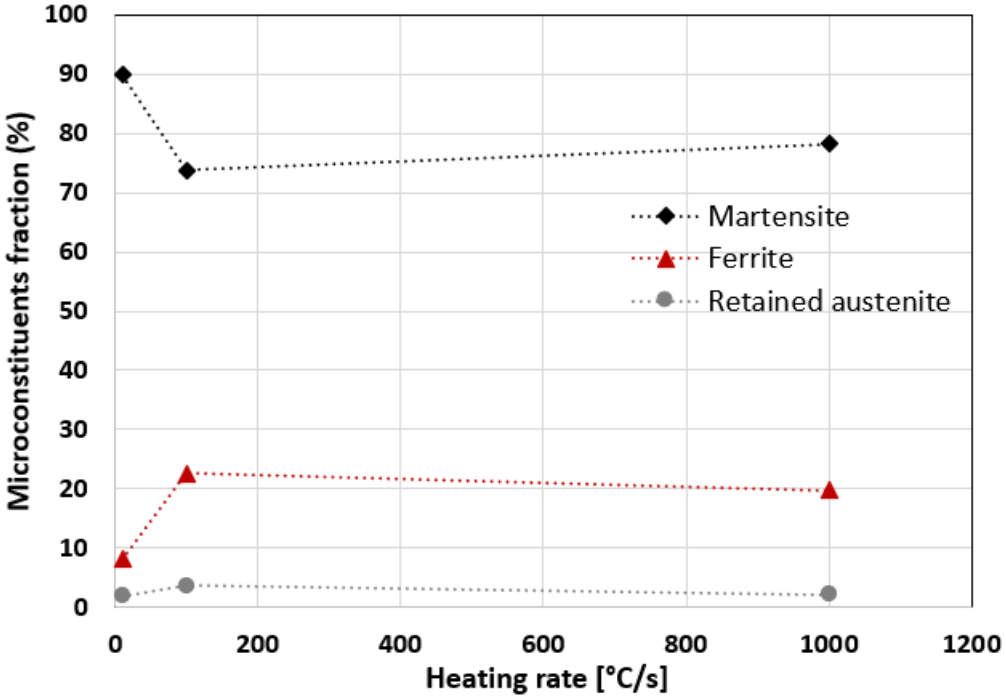

Figure 15. Microstructural evolution at different HRs for peak temperature at Ac3: 950 °C (data from [57]; steel chemical composition: 0.2% C).

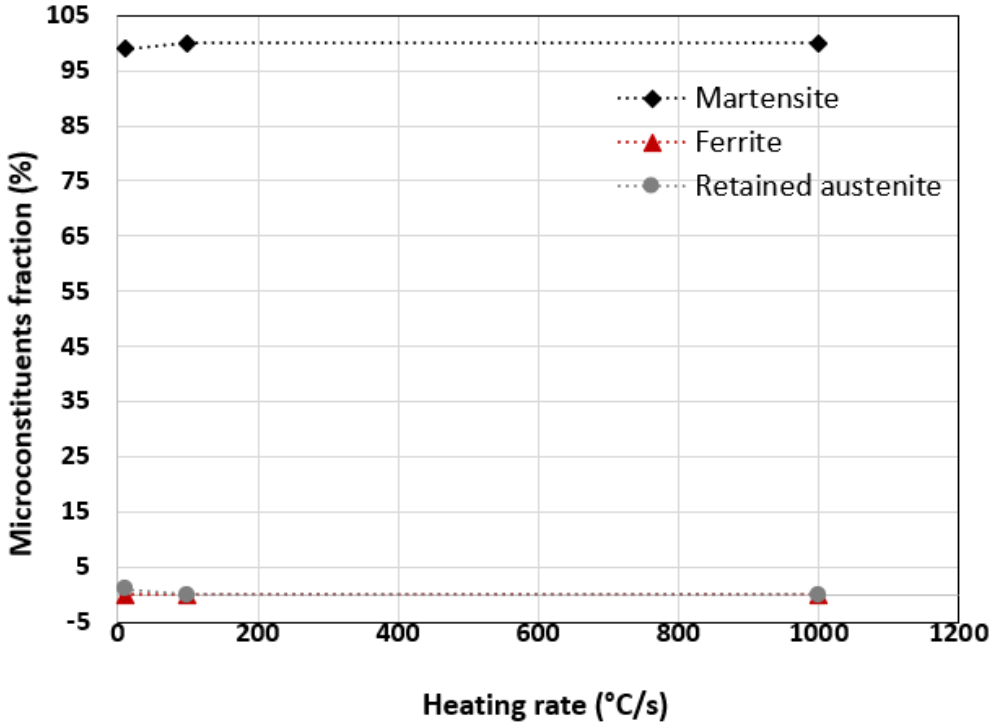

Figure 16. Microstructural evolution at different HRs for peak temperature at Ac3: 950 °C (data from [57]; steel chemical composition: 0.2% C + Mo + Ti + Nb).

The effect of an increased heating rate in reducing the final fraction of martensite at the end of the treatment was apparent at 100 °C/s. Possible reasons to explain why the martensite fraction was generally lower in the low-alloyed steel compared to the alloyed one are, on one hand, the higher critical transformation temperatures and, on the other hand, the lower hardenability. In the former case, the amount of austenite transformed during the process was lower; in the latter case, a lower fraction of the austenite formed at high temperature is converted to martensite during cooling.

6. Effect of UFH on the Textural Evolution and Magnetic Properties of NGO Steels

Nonoriented grain (NGO) electrical steels can be classified as low-C steels, and regarding the microstructural evolution, mechanical properties, and phase transformation temperatures, the effect of UFH can be considered to be similar. In this section, the effect of UFH on the textural evolution and magnetic properties of NGO steels is reported.

For NGO electrical steels, the role of ultrafast annealing on textural evolution is evident, since an increase in the occurrence of Goss component is observed, which leads to an improvement of magnetic properties [61–63].

The magnetic properties of Fe–Si steels strictly depend on textural evolution [64–70], and consequently on the starting microstructure [71–73], annealing conditions [74], and cold-rolling settings [75–80]. Core losses and eddy current losses are strongly dependent on recrystallization and grain size morphology after cold rolling. Grain size and the absence of impurities such as dislocations, grain boundaries, or precipitates are the most important factors determining power losses. The most relevant textural components in electrical steels are the Goss component (110) [001], the rotated Cube component (100) [011], and the γ-fiber [111]//ND [78–82]. After cold rolling, the texture is characterized by very strong Goss and cube component orientations that, in principle, are very positive in terms of magnetic features; in fact, the matrix is highly deformed. However, the effect of the subsequent recrystallization annealing treatment promotes the development of the γ-fiber, the typical recrystallization texture of ferritic steels, and the consequent reduction in deformation components. In conventional industrial lines, the nucleation of textural components starts during the (slow) heating stage and interacts with the concurrent recovery process. There-

fore, since the Goss and Cube components nucleate in high-energy zones of the material, the UFH treatment could represent an opportunity to reduce the undesired effect of recovery, and to produce NGO steels with better textural properties.

Wang et al. [64] explored different heat treatment approaches to optimize the magnetic properties of electrical steels. A cold-rolled NGO steel was subjected to an extremely short annealing cycle in the range of 3–30 s, with heating rates from 15 to 300 °C/s and peak temperature from 880 to 980 °C. The presence of silicon (no less than 1%) increases the critical temperatures of the steel, thus permitting the use of peak temperatures higher than those of the corresponding low-carbon steels. In the case of fast heating, a very strong {110}<001> (Goss) texture develops [64,72]. Its intensity increases with increasing heating rate, but decreases as the annealing time increases. Moreover, in coarse-grained specimens, the Goss component is significantly strengthened, and the {111}<112> component is slightly weakened with increasing heating rate. On the other hand, in a fine-grained specimen, the intensity of the Goss component showed only a slight increase, but the {111}<112> component was greatly reduced.

Generally speaking, as the heating rate increases, the typical recrystallization texture of ferrite (γ-fiber) weakens significantly due to the very short heating treatment, whereas the Goss component is extremely favored. Since the nucleation of the Goss component occurs in regions of the deformed matrix with higher stored energy (namely, shear bands), higher heating rates reduce the negative effect of recovery, thus promoting their nucleation and further growth [65–68,71]. This result is in agreement with the work of Hutchinson [83], who reported a schematic ranking of the nucleation rate of different textural components as a function of time during annealing. In fact, from a kinetic viewpoint, the {110} orientations started nucleating earlier than {111} did, thus exploiting a larger kinetic advantage as the heating rate increased.

Regarding the magnetic properties of NGO electrical steels as a function of heating rate, the following results emerged from the experiments [63,64]:

- Magnetic induction was improved as the HR increased from 15 to 300 °C/s. This was due to the optimized recrystallized texture caused by rapid heating.
- Core losses decreased as the heating rate increased from 15 to 100 °C/s. As a matter of fact, this effect was apparent when the heating rate exceeded 100 °C/s since it was associated with the decrease in mean grain size with increasing HR. Incidentally, this induced a parallel decrease in classical eddy current losses, but an increase in hysteresis losses.
- Annealing treatments up to 850 °C after cold rolling improved the magnetic properties (higher permeability and lower energy losses) due to the increase in grain size and the development of a {100} fiber-type texture.

7. Conclusions

The effect of ultrafast heating on different classes of steel, specifically on medium/low-C, NGO, and stainless steels, was analyzed in this paper with respect to the main metallurgical aspects: phase transformation, recrystallization, mechanical properties, and textural evolution. In particular, the variation trend with heating rate was highlighted, focusing on the main metallurgical properties (phase transformation, recrystallization, and textural evolution) for different classes of materials.

The conclusions can be summarized in the following points:

- The UFH treatment had a strong effect on reducing the grain size, in particular on medium/low-C steels, with a PAG size reduction of 55%, shifting from 10 to 1000 °C/s. Ferritic grains showed a maximal reduction of 76%, increasing from 150 to 1500 °C/s. The effect on the stainless steels was similar but much less pronounced: the average grain size reduction was 10% from 25 to 500 °C/s.
- In medium/low-C steels, with increasing heating rate, critical transformation points Ac1 and Ac3 were shifted towards higher temperatures. Furthermore, the recrystal-

lization temperatures were also shifted towards higher values in both carbon and stainless steels.

- The increase in heating rate produces an improvement of almost all mechanical characteristics. In medium/low-C steels, the comparison of conventional annealing and ultrafast heating showed an increase in UTS and ε_c (about 20% and from 2.6% to 12.8%, respectively); the YS remained at the same level. When UFH was applied to ferritic stainless steels, the annealed strip has comparable mechanical characteristics with those from standard industrial production. In austenitic stainless steels, there was instead an improvement of the uniform elongation from 11% to 37% with increasing heating rate from 2 to 100 °C/s.
- Textural evolution was directly connected to magnetic properties of NGO steels, and higher heating rates promoted the nucleation of Cube and Goss components in the high-stored-energy zones. Annealing time had a significant effect on the occurrence of the Goss component that nucleates at the initial stages of recrystallization. Moreover, a slow heating with a longer recovery phase reduced the intensity of the Goss component, and the overall texture is more random. In terms of magnetic properties, the magnetic induction increased from 15 to 300 °C/s, and core losses decreased in a range of heating rate from 15 to 100 °C/s. In the case of a heating rate greater than 100 °C/s, grain size underwent severe refinement, with a consequent decrease in eddy current losses, and an increase in hysteresis losses.

Author Contributions: Conceptualization, M.G., A.D.S.; methodology, M.G.; formal analysis, M.G., G.S: data curation, M.G., G.S.; writing—original draft preparation, M.G.; writing—review and editing, A.D.S., G.S., G.T., P.E.D.N.; supervision, A.D.S., P.E.D.N.; project administration, L.A. All authors have read and agreed to the published version of the manuscript.

Funding: This research was funded by REGIONE UMBRIA based on *Piano Sviluppo e Coesione FSC ex DGR n. 251/2021*, grant number CUP I42C20001280008.

Institutional Review Board Statement: Not applicable.

Informed Consent Statement: Not applicable.

Data Availability Statement: The data presented in this study are available on request from the corresponding author.

Conflicts of Interest: The authors declare no conflict of interest.

References

1. Funatani, K. Heat treatment of automotive components: Current status and future trends. *Trans. Indian Inst. Met.* **2004**, *57*, 381–396.
2. Naar, R.; Bay, F. Numerical optimisation for induction heat treatment processes. *Appl. Math. Model.* **2013**, *37*, 2074–2085. [CrossRef]
3. Yan, P.; Güngör, O.E.; Thibaux, P.; Liebeherr, M.; Bhadeshia, H.K.D.H. Tackling the toughness of steel pipes produced by high frequency induction welding and heat-treatment. *Mater. Sci. Eng. A* **2011**, *528*, 8492–8499. [CrossRef]
4. Sherman, W. Case hardening by megacycle induction heating. *Trans. Electrochem. Soc.* **1944**, *86*, 247. [CrossRef]
5. Kalpande, S.D. Performance improvement, an induction hardening machine, cycle time, and productivity. *Perform. Improv.* **2007**, *46*, 9–16. [CrossRef]
6. Lolla, T.; Cola, G.; Naraynana, B.; Alexandrov, B.; Babu, S.S. Development of rapid heating and cooling (flash processing) process to produce advanced high strength steel microstructures. *Mater. Sci. Technol.* **2022**, *27*, 863. [CrossRef]
7. Cola, G., Jr. Flash bainite nucleated in 80ms by water quenching, AIST Steel Properties and Applications Conference Proceedings, Combined with Ms and T'07. *Mater. Sci. Technol.* **2007**, *6*, 3845.
8. Jászfi, V.; Prevedel, P.; Eggbauer, A.; Godai, Y.; Raninger, P.; Mevec, D.; Panzenböck, M.; Ebner, R. Influence of the parameters of induction heat treatment on the mechanical properties of 50CrMo4. *HTM J. Heat Treat. Mater.* **2019**, *74*, 366–379. [CrossRef]
9. Honda, T.; Santos, E.C.; Kida, K.; Shibukawa, T. Changes in the microstructure of 13Cr-2Ni-2Mo stainless steels through the quenching process by induction heating. *Int. J. Mater. Prod. Technol.* **2012**, *45*, 31–40. [CrossRef]
10. Markovsky, P.E.; Semiatin, S.L. Tailoring of microstructure and mechanical properties of Ti-6Al-4V with local rapid (induction) heat treatment. *Mater. Sci. Eng. A* **2011**, *528*, 3079–3089. [CrossRef]
11. Napoli, G.; Paura, M.; Vela, T.; Di Schino, A. Colouring titanium alloys by anodic oxidation. *Metalurgija* **2018**, *57*, 111–113.

12. Cunningham, J.L.; Medlin, D.J.; Krauss, G. Effects of induction hardening and prior cold work on a microalloyed medium carbon steel. *J. Mater. Eng. Perform.* **1999**, *8*, 401–408. [CrossRef]
13. Vieweg, A.; Ressel, G.; Prevedel, P.; Marsoner, S.; Ebner, R. Effects of the inductive hardening process on the martensitic structure of a 50CrMo4 steel. *HTM J. Heat Treat. Mater.* **2017**, *72*, 3–9. [CrossRef]
14. Clarke, K.D.; Van Tyne, C.J.; Vigil, C.J.; Hackenberg, R.E. Induction hardening 5150 steel: Effects of initial microstructure and heating rate. *J. Mater. Eng. Perform.* **2011**, *20*, 161–168. [CrossRef]
15. Eggbauer, A.; Lukas, M.; Prevedel, P.; Panzenböck, M.; Ressel, G.; Ebner, R. Effect of Initial Microstructure, Heating Rate, and Austenitizing Temperature on the Subsequent Formation of Martensite and Its Microstructural Features in a QT Steel. *Steel Res. Int.* **2019**, *90*, 1800317. [CrossRef]
16. Roumen, P.; Jurij, S.; Wlodzimierz, K.; Leo, K. Grain refinement of a cold rolled TRIP assisted steel after ultra short annealing. *Mater. Sci. Forum* **2012**, *715–716*, 661–666. [CrossRef]
17. Banis, A.; Bouzouni, M.; Petrov, R.H.; Papaefthymiou, S. Simulation and characterisation of the microstructure of ultra-fast heated dual-phase steel. *Mater. Sci. Technol.* **2020**, *36*, 1282–1291. [CrossRef]
18. Ochi, T.; Koyasu, Y. Strengthening of surface induction hardened parts for automotive shafts subject to torsional load. *SAE Tech. Pap.* **1994**, *103*, 570–580. [CrossRef]
19. Sackl, S.; Leitner, H.; Zuber, M.; Clemens, H.; Primig, S. Induction Hardening vs Conventional Hardening of a Heat Treatable Steel. *Metall. Mater. Trans. A Phys. Metall. Mater. Sci.* **2014**, *45*, 5657–5666. [CrossRef]
20. Castro Cerda, F.M.; Sabirov, I.; Goulas, C.; Sietsma, J.; Monsalve, A.; Petrov, R.H. Austenite formation in 0.2% C and 0.45% C steels under conventional and ultrafast heating. *Mater. Des.* **2017**, *116*, 448–460. [CrossRef]
21. Massardier, V.; Ngansop, A.; Fabregue, D.; Cazottes, S.; Merlin, J. Ultra-rapid intercritical annealing to improve deep drawability of low-carbon, al-killed steels. *Metall. Mater. Trans. A Phys. Metall. Mater. Sci.* **2012**, *43*, 2225–2236. [CrossRef]
22. Valdes-Tabernero, M.A.; Vercruysse, F.; Sabirov, I.; Petrov, R.H.; Monclus, M.A.; Molina-Aldareguia, J.M. Effect of Ultrafast Heating on the Properties of the Microconstituents in a Low-Carbon Steel. *Metall. Mater. Trans. A Phys. Metall. Mater. Sci.* **2018**, *49*, 3145–3150. [CrossRef]
23. Castro Cerda, F.M.; Goulas, C.; Sabirov, I.; Kestens, L.A.I.; Petrov, R.H. The effect of the pre-heating stage on the microstructure and texture of a cold rolled FeCMnAlSi steel under conventional and ultrafast heating. *Mater. Charact.* **2017**, *130*, 188–197. [CrossRef]
24. Castro, N.A.; de Campos, M.F.; Landgraf, F.J.G. Effect of deformation and annealing on the microstructure and magnetic properties of grain-oriented electrical steels. *J. Magn. Magn. Mater.* **2006**, *304*, 617–619. [CrossRef]
25. Bacaltchuk, C.M.B.; Castello-Branco, G.A.; Garmestani, H.; Rollett, A.D. Effect of magnetic field during secondary annealing on texture and microstructure of nonoriented silicon steel. *Mater. Manuf. Process.* **2004**, *19*, 611–617. [CrossRef]
26. Di Schino, A.; Testani, C. Corrosion behaviour and mechanical properties of AISI 316 stainless steels clad Q235 plate. *Metals* **2020**, *10*, 552. [CrossRef]
27. Di Schino, A.; Gaggiotti, M.; Testani, C. Heat treatmemnt effect on microstructure evolution in a 7% Cr steel for forging. *Metals* **2020**, *10*, 808. [CrossRef]
28. Stornelli, G.; Montanari, R.; Testani, C.; Pilloni, L.; Napoli, G.; Di Pietro, O.; Di Schino, A. Microstructure refinement effect on EUROFER 97 steel for nuclear fusion application. *Mater. Sci. Forum* **2021**, *1016*, 1392–1397. [CrossRef]
29. Stornelli, G.; Gaggia, D.; Rallini, M.; Di Schino, A. Heat Treatment Effect on Maraging Steel Manufactured by Laser Powder Bed Fusion Technology: Microstructure and Mechanical Properties. *Acta Metall. Slovaca* **2021**, *27*, 122–126. [CrossRef]
30. Stornelli, G.; Gaggiotti, M.; Mancini, S.; Napoli, G.; Rocchi, C.; Tirasso, C.; Di Schino, A. Recrystallization and Grain Growth of AISI 904L Super-Austenitic Stainless Steel: A Multivariate Regression Approach. *Metals* **2022**, *12*, 200. [CrossRef]
31. Masumura, T.; Seto, Y.; Tsuchiyama, T.; Kimura, K. Work-hardening mechanism in high-nitrogen austenitic stainless steel. *Mater. Trans.* **2020**, *61*, 678–684. [CrossRef]
32. Mallick, P.; Tewary, N.K.; Ghosh, S.K.; Chattopadhyay, P.P. Effect of cryogenic deformation on microstructure and mechanical properties of 304 austenitic stainless steel. *Mater. Charact.* **2017**, *133*, 77–86. [CrossRef]
33. Humphreys, F.J.; Hatherly, M. Grain Growth Following Recrystallization. In *Recrystallization and Related Annealing Phenomena*; Elsevier: Oxford, UK, 2004; pp. 333–378. [CrossRef]
34. Di Schino, A.; Kenny, J.M. Effects of the grain size on the corrosion behavior of refined AISI 304 stainless steel. *J. Mater. Sci. Lett.* **2002**, *21*, 1631–1634. [CrossRef]
35. Sinclair, C.W.; Mithieux, J.D.; Schmitt, J.H.; Bréchet, Y. Recrystallization of stabilized ferritic stainless steel sheet. *Metall. Mater. Trans. A Phys. Metall. Mater. Sci.* **2005**, *36*, 3205–3215. [CrossRef]
36. Belyakov, A.; Kimura, Y.; Tsuzaki, K. Recovery and recrystallization in ferritic stainless steel after large strain deformation. *Mater. Sci. Eng. A* **2005**, *403*, 249–259. [CrossRef]
37. Callister, W.D. *Scienza e Ingegneria dei Materiali*; Polytechnic University of Milan: Milan, Italy, 1999.
38. Gao, N.; Baker, T.N. Austenite Grain Growth Behaviour of Microalloyed Al-V-N and Al-V-Ti-N Steels. *ISIJ Int.* **1998**, *38*, 744–751. [CrossRef]
39. Gavard, L.; Montheillet, F.; Coze, J. Le recrystallization and grain growth in high purity austenitic stainless steels. *Scr. Mater.* **1998**, *39*, 1095–1099. [CrossRef]

40. De Knijf, D.; Puype, A.; Föjer, C.; Petrov, R. The influence of ultra-fast annealing prior to quenching and partitioning on the microstructure and mechanical properties. *Mater. Sci. Eng. A* **2015**, *627*, 182–190. [CrossRef]
41. Meng, Q.; Li, J.; Zheng, H. High-efficiency fast-heating annealing of a cold-rolled dual-phase steel. *Mater. Des.* **2014**, *58*, 194–197. [CrossRef]
42. Castro Cerda, F.M.; Kestens, L.A.I.; Monsalve, A.; Petrov, R.H. The effect of ultrafast heating in cold-rolled low carbon steel: Recrystallization and texture evolution. *Metals* **2016**, *6*, 288. [CrossRef]
43. Banis, A.; Duran, E.H.; Bliznuk, V.; Sabirov, I.; Petrov, R.H.; Papaefthymiou, S. The effect of ultra-fast heating on the microstructure, grain size and texture evolution of a commercial low-c, medium-Mn DP steel. *Metals* **2019**, *9*, 877. [CrossRef]
44. Sun, G.S.; Hu, J.; Zhang, B.; Du, L.X. The significant role of heating rate on reverse transformation and coordinated straining behavior in a cold-rolled austenitic stainless steel. *Mater. Sci. Eng. A* **2018**, *732*, 350–358. [CrossRef]
45. Jaskari, M.; Järvenpää, A.; Karjalainen, P. The effect of heating rate and temperature on microstructure and r-value of type 430 ferritic stainless steel. *Mater. Sci. Forum* **2018**, *941*, 364–369. [CrossRef]
46. Di Schino, A. Analysis of phase transformation in high strength low alloyed steels. *Metalurgija* **2017**, *56*, 349–352.
47. Castro Cerda, F.M.; Schulz, B.; Celentano, D.; Monsalve, A.; Sabirov, I.; Petrov, R.H. Exploring the microstructure and tensile properties of cold-rolled low and medium carbon steels after ultrafast heating and quenching. *Mater. Sci. Eng. A* **2019**, *745*, 509–516. [CrossRef]
48. Valdes-Tabernero, M.A.; Celada-Casero, C.; Sabirov, I.; Kumar, A.; Petrov, R.H. The effect of heating rate and soaking time on microstructure of an advanced high strength steel. *Mater. Charact.* **2019**, *155*, 109822. [CrossRef]
49. Senuma, T.; Kawasaki, K.; Takemoto, Y. Recrystallization behavior and texture formation of rapidly annealed cold-rolled extralow carbon steel sheets. *Mater. Trans.* **2006**, *47*, 1769–1775. [CrossRef]
50. Samei, J.; Zhou, L.; Kang, J.; Wilkinson, D.S. Microstructural analysis of ductility and fracture in fine-grained and ultrafine-grained vanadium-added DP1300 steels. *Int. J. Plast.* **2018**, *117*, 58–70. [CrossRef]
51. Speer, J.; Matlock, D.K.; De Cooman, B.C.; Schroth, J.G. Carbon partitioning into austenite after martensite transformation. *Acta Mater.* **2003**, *51*, 2611–2622. [CrossRef]
52. Sharma, D.K.; Filipponi, M.; Di Schino, A.; Rossi, F.; Castaldi, J. Corrosion behaviour of high temperature fuel cells: Issues for materials selection. *Metalurgija* **2019**, *58*, 347–351.
53. Lebedev, A.A.; Kosarchuk, V.V. Influence of phase transformations on the mechanical properties of austenitic stainless steels. *Int. J. Plast.* **2000**, *16*, 749–767. [CrossRef]
54. Jiang, Y.; Tan, H.; Wang, Z.; Hong, J.; Jiang, L.; Li, J. Influence of Creq/Nieq on pitting corrosion resistance and mechanical properties of UNS S32304 duplex stainless steel welded joints. *Corros. Sci.* **2013**, *70*, 252–259. [CrossRef]
55. Nakagawa, H.; Miyazaki, T. Effects of the amount of retained austenite on the microstructures and mechanical properties of a precipitation hardening martensitic stainless steel. *Tetsu-to-Hagane/J. Iron Steel Inst. Jpn.* **1998**, *84*, 43–48. [CrossRef]
56. Stornelli, G.; Schino, A.D.; Mancini, S.; Montanari, R.; Testani, C.; Varone, A. Applied sciences Grain Refinement and Improved Mechanical Properties of EUROFER97 by Thermo-Mechanical Treatments. *Appl. Sci.* **2021**, *11*, 10598. [CrossRef]
57. Hernandez-Duran, E.I.; Corallo, L.; Ros-Yanez, T.; Castro-Cerda, F.M.; Petrov, R.H. Influence of Mo–Nb–Ti additions and peak annealing temperature on the microstructure and mechanical properties of low alloy steels after ultrafast heating process. *Mater. Sci. Eng. A* **2021**, *808*, 140928. [CrossRef]
58. Papaefthymiou, S.; Bouzouni, M.; Petrov, R.H. Study of carbide dissolution and austenite formation during ultra–fast heating in medium carbon chromium molybdenum steel. *Metals* **2018**, *8*, 646. [CrossRef]
59. Roumen, P.; Farideh, H.; Jurij, S.; Jesus, M.; Sietsma, J.; Kestens, L. Ultra-Fast Annealing of High Strength Steel. *Int. Virtual J. Mach. Technol. Mater.* **2012**, *8*, 68–71.
60. Salvatori, I.; Moore, W.B.R. Ultra rapid annealing of cold rolled stainless steels. *ISIJ Int.* **2000**, *40*, 79–83. [CrossRef]
61. Wu, S.Y.; Lin, C.H.; Hsu, W.C.; Chang, L.; Sun, P.L.; Kao, P.W. Effect of heating rate on the development of annealing texture in a 1.09 wt. % Si non-oriented electrical steel. *ISIJ Int.* **2016**, *56*, 326–334. [CrossRef]
62. Iordache, V.E.; Hug, E. Effect of mechanical strains on the magnetic properties of electrical steels. *J. Optoelectron. Adv. Mater.* **2004**, *6*, 1297–1303.
63. Gutiérrez, C.E.; Salinas-Rodríguez, A.; Nava-Vázquez, E. Effect of Fast Annealing on Microstructure and Mechanical Properties of Non-Oriented Al-Si Low C Electrical Steels. *Mater. Sci. Forum* **2007**, *560*, 29–34. [CrossRef]
64. Wang, J.; Li, J.; Mi, X.; Zhang, S.; Volinsky, A.A. Rapid Annealing effects on microstructure, texture, and magnetic properties of non-oriented electrical steel. *Met. Mater. Int.* **2012**, *18*, 531–537. [CrossRef]
65. Gutiérrez-Castañeda, E.J.; Salinas-Rodríguez, A. Effect of annealing prior to cold rolling on magnetic and mechanical properties of low carbon non-oriented electrical steels. *J. Magn. Magn. Mater.* **2011**, *323*, 2524–2530. [CrossRef]
66. Malin, A.S.; Hatherly, M. Shear bands in deformed metals. *Scr. Metall.* **1984**, *13*, 576.
67. Wei, Q.; Jia, D.; Ramesh, K.T.; Ma, E. Evolution and microstructure of shear bands in nanostructured Fe. *Appl. Phys. Lett.* **2002**, *81*, 1240–1242. [CrossRef]
68. Cerda, F.C.; Goulas, C.; Sabirov, I.; Papaefthymiou, S.; Monsalve, A.; Petrov, R.H. Microstructure, texture and mechanical properties in a low carbon steel after ultrafast heating. *Mater. Sci. Eng. A* **2016**, *672*, 108–120. [CrossRef]
69. Stornelli, G.; Faba, A.; Di Schino, A.; Folgarait, P.; Ridolfi, M.R.; Cardelli, E.; Montanari, R. Properties of additively manufactured electric steel powder cores with increased Si content. *Materials* **2021**, *14*, 1489. [CrossRef]

70. Stornelli, G.; Ridolfi, M.R.; Folgarait, P.; De Nisi, J.; Corapi, D.; Repitsch, C.; Di Schino, A. Feasibility assessment of magnetic cores through additive manufacturing techniques. *Metall. Ital.* **2021**, *2*, 50–63.
71. Ray, R.K.; Jonas, J.J.; Hook, R.E. *Cold Rolling and Annealing Textures in Low Carbon and Extra Low Carbon Steels*; Taylor & Francis: Abingdon, UK, 1994; Volume 39.
72. Park, J.T.; Szpunar, J.A. Evolution of recrystallization texture in nonoriented electrical steels. *Acta Mater.* **2003**, *51*, 3037–3051. [CrossRef]
73. Park, J.T.; Szpunar, J.A. Effect of initial grain size on texture evolution and magnetic properties in nonoriented electrical steels. *J. Magn. Magn. Mater.* **2009**, *321*, 1928–1932. [CrossRef]
74. Oldani, C.; Silvetti, S.P. Microstructure and texture evolution during the annealing of a lamination steel. *Scr. Mater.* **2000**, *43*, 129–134. [CrossRef]
75. Wei, X.; Hojda, S.; Dierdorf, J.; Lohmar, J.; Hirt, G. Model for texture evolution in cold rolling of 2.4 wt.-% Si non-oriented electrical steel. In *AIP Conference Proceedings*; AIP Publishing LLC: Melville, NY, USA, 2017; Volume 1896. [CrossRef]
76. Stojakovic, D. Microstructure Evolution in Deformed and Recrystallized Electrical Steel. Ph.D. Thesis, Drexel University, Philadelphia, PA, USA, March 2008.
77. Salih, M.Z.; Weidenfeller, B.; Al-Hamdany, N.; Brokmeier, H.G.; Gan, W.M. Magnetic properties and crystallographic textures of Fe 2.6% Si after 90% cold rolling plus different annealing. *J. Magn. Magn. Mater.* **2014**, *354*, 105–111. [CrossRef]
78. Silva, J.M.; Baêta Júnior, E.S.; Moraes, N.R.D.C.; Botelho, R.A.; Felix, R.A.C.; Brandao, L. Influence of different kinds of rolling on the crystallographic texture and magnetic induction of a NOG 3 wt% Si steel. *J. Magn. Magn. Mater.* **2017**, *421*, 103–107. [CrossRef]
79. Kestens, L.; Aernoudt, E.; Dilewijns, J.; Leuven, K.U.; Metallurgy, P.; Sidmar, N. V The effect of cross rolling on texture and magnetic. *Textures Microstruct.* **1991**, *14*, 921–926.
80. Kvackaj, T.; Bidulska, J.; Biduslky, R. Overview of HSS Steel Grades Development and Study of Reheating Condition Effects on Austenite Grain Size Changes. *Materials* **2021**, *14*, 1988. [CrossRef]
81. Di Pietro, O.; Napoli, G.; Gaggiotti, M.; Marini, R.; Stornelli, G.; Di Schino, A. Analysis of plastic forming paramaters in AISI 441 stainless steels. *Acta Metall. Slov.* **2020**, *26*, 178–183. [CrossRef]
82. Di Schino, A. Precipitation state of warm worked AA7050 alloy: Effect on toughness behavior. *Acta Metall. Slov.* **2021**, *27*, 53–56. [CrossRef]
83. Hutchinson, W.B. Development of textures in recrystallization. *Met. Sci.* **1974**, *8*, 185–196. [CrossRef]